Article published online: 2024-11-26

A Predictive Model Integrating AI Recognition Technology and Biomarkers for Lung Nodule Assessment

Tao Zhou[1] Ping Zhu[1] Kaijian Xia[1] Benying Zhao[1]

[1] Department of Cardiothoracic Surgery, Changshu Hospital Affiliated to Soochow University, Changshu, China

Thorac Cardiovasc Surg

Address for correspondence Tao Zhou, MD, Department of Cardiothoracic Surgery, Changshu Hospital Affiliated to Soochow University, No. 1, Shuyuan Street, Changshu 215500, China (e-mail: zhoutao10052024@163.com).

Abstract

Background Lung cancer is the most prevalent and lethal cancer globally, necessitating accurate differentiation between benign and malignant pulmonary nodules to guide treatment decisions. This study aims to develop a predictive model that integrates artificial intelligence (AI) analysis with biomarkers to enhance early detection and stratification of lung nodule malignancy.

Methods The study retrospectively analyzed the patients with pathologically confirmed pulmonary nodules. AI technology was employed to assess CT features, such as nodule size, solidity, and malignancy probability. Additionally, lung cancer blood biomarkers were measured. Statistical analysis involved univariate analysis to identify significant differences among factors, followed by multivariate logistic regression to establish independent risk factors. The model performance was validated using receiver operating characteristic curves and decision curve analysis (DCA) for internal validation. Furthermore, an external dataset comprising 51 cases of lung nodules was utilized for independent validation to assess robustness and generalizability.

Results A total of 176 patients were included, divided into benign/preinvasive ($n = 76$) and invasive cancer groups ($n = 100$). Multivariate analysis identified eight independent predictors of malignancy: lobulation sign, bronchial inflation sign, AI-predicted malignancy probability, nodule nature, diameter, solidity proportion, vascular endothelial growth factor, and lung cancer autoantibodies. The combined predictive model demonstrated high accuracy (area under the curve [AUC] = 0.946). DCA showed that the combined model significantly outperformed the traditional model, and also proved superior to models using AI-predicted malignancy probability or the seven lung cancer autoantibodies plus traditional model. External validation confirmed its robustness (AUC = 0.856), achieving a sensitivity of 0.80 and specificity of 0.86, effectively distinguishing between invasive and noninvasive nodules.

Conclusion This combined approach of AI-based CT features analysis with lung cancer biomarkers provides a more accurate and clinically useful tool for guiding treatment decisions in pulmonary nodule patients. Further studies with larger cohorts are warranted to validate these findings across diverse patient populations.

Keywords
- pulmonary nodules
- artificial intelligence recognition
- lung cancer biomarker
- predictive model

received
May 7, 2024
accepted after revision
October 1, 2024
accepted manuscript online
October 22, 2024

DOI https://doi.org/10.1055/a-2446-9832.
ISSN 0171-6425.

Georg Thieme Verlag KG, Rüdigerstraße 14, 70469 Stuttgart, Germany

Introduction

Lung cancer stands as the most prevalent and fatal malignancy worldwide, with its incidence and mortality rates steadily climbing in China.[1,2] Timely diagnosis and treatment significantly impact patient outcomes,[3] yet accurately distinguishing between nodules requiring intervention and those that do not remains a challenge. Historically, clinical judgment has guided the assessment of pulmonary nodules, but this approach has resulted in overtreatment, particularly with pure ground glass nodules.[4] Thus, the imperative to balance timely intervention with avoiding unnecessary treatment persists. The emergence of artificial intelligence (AI) recognition software systems offers promise in swiftly and precisely identifying lung nodules and assessing their malignancy potential based on various characteristics and ancillary data. However, some domestic scholars have highlighted limitations in sensitivity, specificity, and overall agreement rates of AI imaging systems, with elevated misdiagnosis rates.[5] Concurrently, studies have revealed the detection of lung cancer autoantibodies months to years prior to cancer diagnosis through imaging modalities. Notably, research by Trudgen K.[6] at the Mayo Clinic in 2014 demonstrated that lung cancer autoantibody profiles could identify stage I lung cancer and provide early warning signs of lung cancer symptoms up to 5 years earlier than imaging, aiding in early detection and risk stratification.[6] Nevertheless, evolving perspectives on the management of ground glass nodules underscore the need for refined approaches. Some experts, following the WHO's fifth edition of chest tumor classification, argue that in situ cancer should not be considered malignant and, thus, does not necessitate surgical resection.[7] Proposing a novel strategy, we advocate for leveraging AI recognition technology to analyze CT features and predict malignancy probability, integrated with lung cancer autoantibodies, tumor markers, and other factors, to establish a predictive model for tumor malignancy and infiltration depth. Such an approach aims to empower clinicians with data-driven insights to make informed treatment decisions, ultimately enhancing patient outcomes. Hence, this study was undertaken.

Materials and Methods

Study Design and Population

Retrospective collection and analysis were conducted on patients who underwent surgery, using Shenrui Medical's AI recognition technology combined with seven types of lung cancer autoantibodies for analysis.

Inclusion criteria

All enrolled patients must have chest CT results confirming the presence of pulmonary nodules without any clinical or drug intervention; after performing chest CT, clear pathological results proving the presence of benign or malignant nodules; age $\geq$18 years; liver function (values of aspartate aminotransferase and alanine aminotransferase are below 2.5 times the maximum normal value), renal function, and heart function are normal; no functional damage to other major organs; and no other primary malignant tumors.

Exclusion criteria

Those who have undergone chest CT and indeed have pulmonary nodules but no pathological examination; patients who have undergone clinical and medication interventions before undergoing blood sampling; patients with rheumatic immune-related diseases; severe hemolysis or high blood lipids $\geq$18.75 mmol/L, high concentration of bilirubin $\geq$573.5 µmol/L; acute or chronic infection; other lung metastases from tumors; and have a history of mental illness.

According to the inclusion and exclusion criteria, a total of 176 cases were included in this study during this time period, including 67 males and 109 females, with an average age of 60 years and a median age of 61 years. All cases had clear pathological types and clinical stages, including 40 benign nodules, 36 preinvasive lesions (8 atypical adenomatous hyperplasia [AAH], 26 in situ carcinoma), 40 minimally invasive adenocarcinoma, and 60 invasive adenocarcinoma. patient CT data were imported into Shenrui Medical's AI recognition technology system, automatically calculating and giving output of the nature, diameter, proportion of solid components, average CT value, as well as the presence or absence of features such as lobulation, speculation, pleural depression, and vascular penetration of pulmonary nodules. At the same time, the malignancy probability of the nodules was judged based on the above features and classified as high-risk nodules if they were greater than 50%. Seven types of lung cancer autoantibodies and tumor marker values were collected from the blood samples, mainly, including neuron-specific enolase (NSE), carcinoembryonic antigen (CEA), cytokeratin fragment (CY211), squamous cell carcinoma antigen (SCC), Pro-Gastrin-Releasing Peptide (Pro-GRP), and vascular endothelial growth factor (VEGF).

Spiral CT Examination Methods and Artificial Intelligence Analysis of Pulmonary Nodules

Siemens 64-row CT machine was used for routine chest CT scanning, with the patient in a supine position and the scanning range from the apex of the lung to below the costophrenic angle at the bottom of the lung. All images were reconstructed through thin-layer postprocessing. patient CT data were imported into Shenrui Medical's AI recognition technology system, automatically calculating and giving output of the nature, diameter, proportion of solid components, average CT value, as well as the presence or absence of features such as lobulation, speculation, pleural depression, and vascular penetration of pulmonary nodules. At the same time, the malignancy probability of the nodules was judged based on the above features and classified as high-risk nodules if they were greater than 50%.

Detection Methods and Evaluation Criteria for Lung Cancer Autoantibodies

Peripheral venous blood samples were collected from preoperative or preoperative fasting patients, and the serum

was centrifuged and separated. Enzyme-linked immunosorbent assay (ELISA) was used to detect autoantibodies against proteins encoded by the tumor suppressor gene *TP53, PGP9.5* (protein gene product 9.5), *SOX2* (sex-determining region Y-box 2), *GAGE7* (G antigen 7), *GBU4-5* (RNA helicase-related antigen 4-5), *MAGEA1* (melanoma antigen A1), and *CAGE* (cancer-associated gene) in the serum. Normal reference value range: p53 <13.09 U/mL, PGP9.5 <11.1 U/mL, SOX2 <10.26 U/mL, GAGE7 <14.36 U/mL, GBU4-5 <6.99 U/mL, MAGEA1 <11.92 U/mL, and CAGE <7.23 U/mL. If the test result exceeds the reference range, it is judged as positive. If any test result is positive, it means that the test results for seven types of lung cancer autoantibodies are judged as positive.[8]

Statistical Analysis

For continuous variables that conform to normality and have uniform variance, an independent sample *t*-test is used. For variables that do not conform to normality, a nonparametric Mann–Whitney U test is used. For categorical variables, the chi-square test is used. Univariate analysis was conducted on 21 factors including gender, age, nodule nature, nodule diameter, CT features, combined detection of lung cancer, CEA, etc. A p-value <0.05 was considered statistically significant. Data with statistically significant differences were included in the results of univariate analysis into multivariate analysis to identify independent risk factors for pulmonary nodule infiltration. a tumor infiltration probability prediction model was established, receiver operating characteristic (ROC) curves were drawn, the area under the curve (AUC) was calculated, the diagnostic cutoff value of the model was determined, and the sensitivity and specificity of the model were analyzed. AUC between 0.5 and 0.7 indicates a low diagnostic value, 0.7 to 0.9 indicates a moderate diagnostic value, and >0.9 indicates a high diagnostic value. p-Value ≤0.05 indicates a statistically significant difference. At the same time, in order to prevent false positive and false negative results and better evaluate the clinical utility of the prediction model, we drew a clinical decision curve analysis (DCA). In addition to the internal cohort, a separate external dataset comprising multiple categories of lung nodules was used to validate the prediction model.

Results

A cohort of 176 patients was enrolled in the study, stratified according to the WHO classification criteria. Patients were categorized into two groups: those with benign or preinvasive lesions not necessitating surgical intervention, encompassing AAH and adenocarcinoma in situ (AIS); and those with invasive cancers warranting surgical management, including microinvasive carcinoma. There were a total of 76 cases in the benign/preinvasive lesion group, including 29 males and 47 females, with an average age of (56.36 ± 13.325) years. There are a total of 100 cases of invasive cancer, including 39 males and 61 females, with an average age of (61.53 ± 11.298) years. Detailed CT features, tumor indicators, and the outcomes of seven lung cancer autoantibodies are summarized in ►**Table 1**.

Following univariate analysis, significant differences were observed between the benign/preinvasive lesion group and the invasive lesion group in several parameters, including age ($p = 0.012$), spiculation ($p < 0.001$), pleural depression ($p = 0.005$), bronchial inflation sign ($p < 0.001$), lobulation sign ($p < 0.001$), nodular ground glass ($p < 0.001$), partial solidity ($p = 0.037$), AI-predicted malignancy probability ($p < 0.001$), average CT value ($p = 0.043$), nodule diameter ($p = 0.038$), solidity proportion ($p < 0.001$), VEGF ($p = 0.017$), and the seven lung cancer autoantibodies ($p < 0.001$). Conversely, no statistically significant differences were noted in gender ($p = 0.91$), vacuolar sign ($p = 0.429$), vascular penetration ($p = 0.168$), CEA ($p = 0.17$), CY211 ($p = 0.566$), NSE ($p = 0.862$), SCC ($p = 0.762$), and Pro-GRP ($p = 0.475$).

Multivariate analysis via binary logistic regression revealed that lobulation sign ($p = 0.004$), bronchial inflation sign ($p = 0.003$), AI-predicted malignancy probability ($p < 0.001$), nodule nature as partially solid ($p < 0.001$), nodule diameter ($p = 0.001$), the proportion of solid ($p < 0.001$), VEGF ($p = 0.008$), and seven autoantibodies of lung cancer ($p = 0.002$) were independent risk factors affecting the pathological characteristics of lung nodules, as shown in ►**Fig. 1**. Based on the results of multiple factor analysis, we established a joint prediction model (group—lobulation sign + bronchial inflation sign + malignant probability + partial solidity + nodule diameter + solidity proportion + VEGF + lung cancer seven joint detections). The formula of this model is logit (P) = −8.829 + 2.593 * lobed sign + 2.055 * bronchial inflation sign + 0.05 * malignant probability + 3.274 * partial solid −1.129 * nodule diameter + 5.936 * solid proportion + 0.008 * VEGF + 1.743 * lung cancer seven joint detections, and compared with the traditional model (group—lobed sign + bronchial inflation sign + partial solidity + nodule diameter + solid proportion + VEGF). At the same time, AI prediction of malignant probability, nodule diameter, and solid proportion are plotted. The ROC curves of VEGF and prediction model have AUCs of 0.760, 0.591, 0.718, 0.605, and 0.946, respectively, as shown in ►**Fig. 2**. The AUC of the combined prediction model can reach 0.946 and achieve a sensitivity of 0.80 and a specificity of 0.86. At the same time, to prevent false positive and false negative results and better evaluate the clinical utility of the prediction model, we plotted the clinical decision curve DCA, as shown in ►**Fig. 3**. According to the DCA curve, compared with the traditional model, the net reclassification index p-value is less than 0.05, indicating a statistical difference, specifying that the joint model is significantly better than the traditional model. The joint model improved by 0.3432 compared to the traditional model, and the comprehensive discrimination improvement index p-value is less than 0.05, indicating a statistical difference. At the same time, we subdivided the model validation and evaluated the advantages and disadvantages of AI prediction of malignancy probability, seven autoantibodies of lung cancer, and their combination. According to the DCA curve, the combined model is also significantly better than AI prediction of malignancy probability or seven autoantibodies of lung cancer + traditional models, as shown in ►**Fig. 4**, indicating that AI recognition technology combined with seven autoantibodies of lung

Table 1 Univariate analysis of pathological characteristics of pulmonary nodules

Variable name	Benign/Preinvasive ($n=76$)	Invasive ($n=100$)	Z-value/χ^2	*p*-value
Age	56.36 (47.00, 67.00)	61.53 (55, 70)	−2.51	0.012
Gender			0.013	0.91
Female	47 (26.7)	61 (34.7)		
Male	29 (16.5)	39 (22.2)		
Emphysema sign	19 (10.8)	20 (11.4)	0.626	0.429
Spiculation sign	27 (15.3)	71 (40.3)	22.020	<0.001
Lobulation sign	5 (2.8)	29 (16.5)	13.927	<0.001
Vascular penetration	54 (30.7)	80 (45.5)	1.903	0.168
Pleural retraction	27 (15.3)	57 (32.4)	7.981	0.005
Bronchial inflation sign	5 (2.8)	39 (22.2)	24.208	<0.001
Ground glass opacity	33 (18.8)	12 (6.8)	22.402	<0.001
Part-solid	19 (10.8)	40 (22.7)	4.360	0.037
Malignancy probability	59.237 (18.00, 88.75)	81.91 (82.25, 90.00)	−5.956	<0.001
Mean CT value	−341.205 (−563.525, −50.875)	−251.821 (−495.45, −12.025)	−2.021	0.043
Nodule diameter	1.389 (0.725, 1.80)	1.574 (0.8, 2.0)	−2.071	0.038
Solid component ratio	0.411 (0.00, 1.00)	0.756 (0.6, 1.0)	−5.147	<0.001
Vascular endothelial growth factor	120.00 (58.518, 151.470)	156.017 (73.98, 206.05)	−2.389	0.017
CEA	2.389 (1.483, 2.938)	3.40 (1.560, 3.415)	−1.372	0.17
CY211	1.920 (1.335, 2.303)	2.113 (1.310, 2.495)	−0.573	0.566
NSE	13.426 (11.615, 14.923)	13.579 (11.735, 14.745)	−0.173	0.862
SCC	0.758 (0.50, 0.90)	0.86 (0.5, 1.0)	−0.303	0.762
Pro-GRP	37.549 (28.008, 42.933)	37.312 (29.615, 43.6275)	−0.714	0.475
Combined detection of seven lung cancer biomarkers	13 (7.4)	47 (26.7)	17.175	<0.001

Abbreviations: CEA, carcinoembryonic antigen; CYFRA21-1, cytokeratin 19 fragment; NSE, neuron-specific enolase; Pro-GRP, pro-gastrin-releasing peptide; SCC, squamous cell carcinoma antigen.

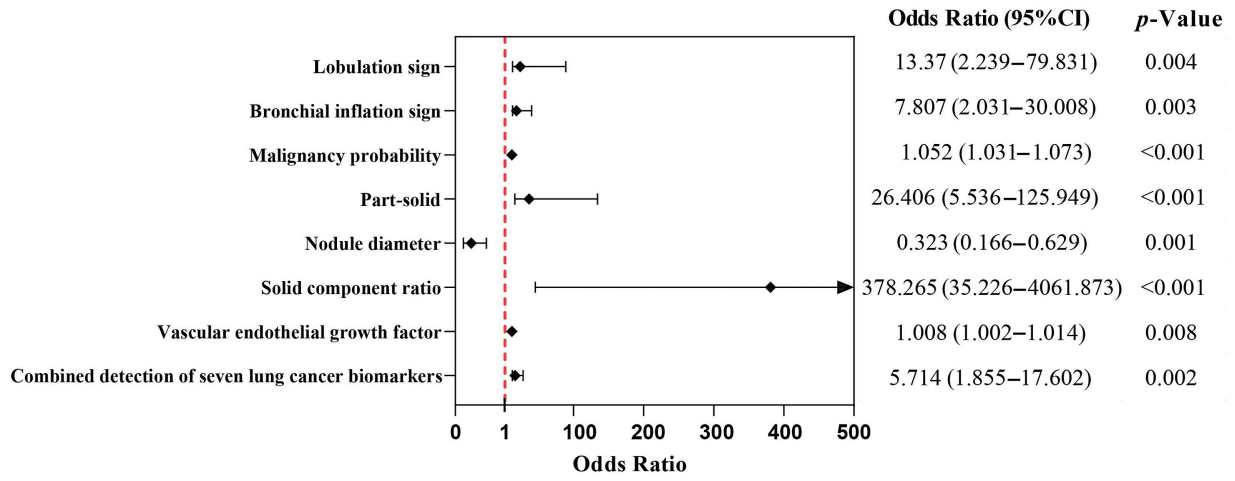

Fig. 1 Forest plot of multivariate analysis for predicting lung nodule malignancy. The figure illustrates the odds ratios (ORs) with 95% confidence intervals for the eight independent predictors of malignancy, identified through multivariate logistic regression analysis. The x-axis represents the ORs on a logarithmic scale, with the red dashed line indicating an OR of 1 (no effect). Larger OR values indicate stronger predictive power, with significant *p*-values (<0.05).

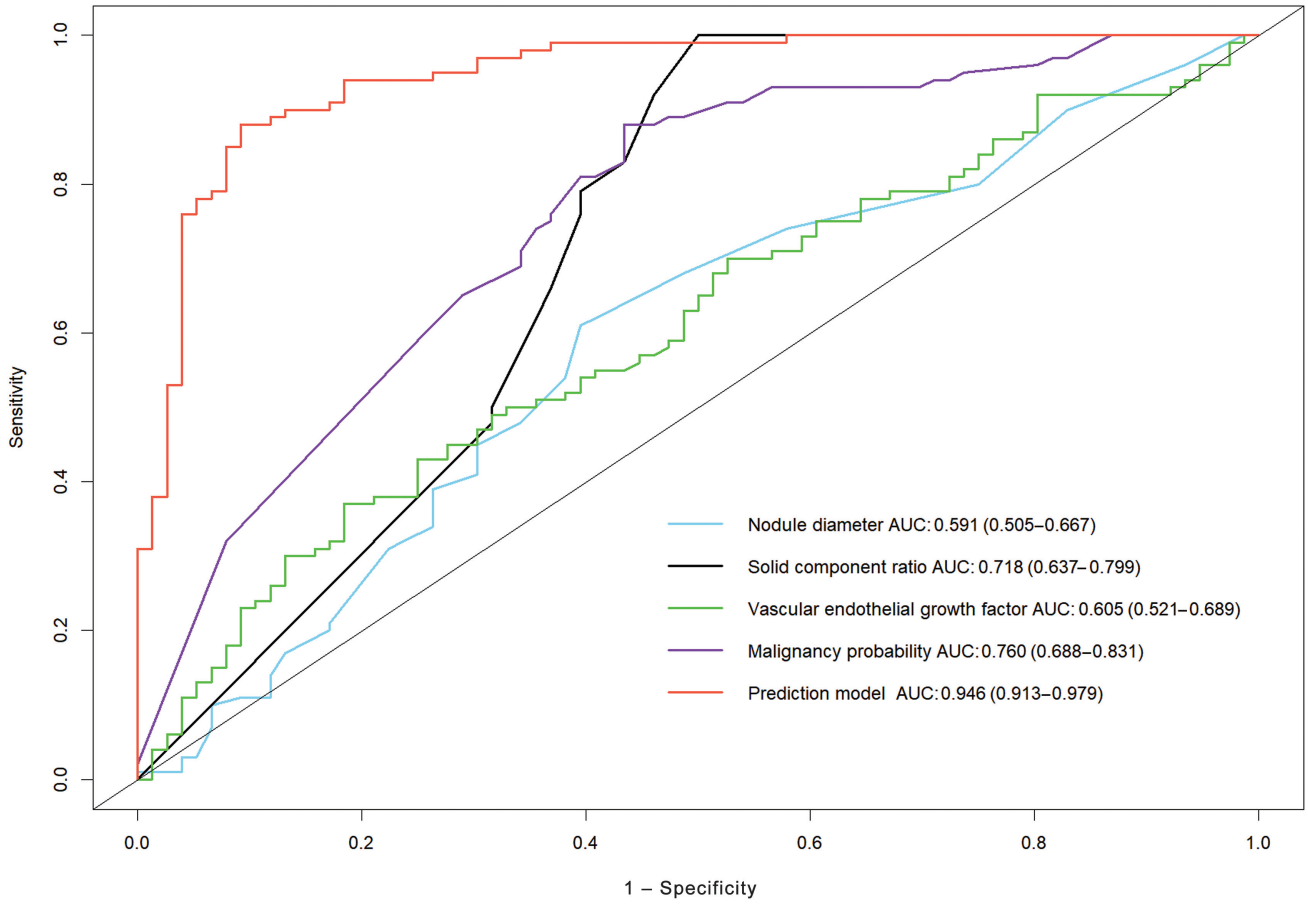

Fig. 2 ROC curves comparing the predictive power of individual features and the combined prediction model. The ROC curves show the predictive accuracy of various features and the combined prediction model for distinguishing lung nodule malignancy. The areas under the curve (AUCs) with 95% confidence intervals (CIs) are provided for each feature. The combined prediction model (red curve) demonstrates the highest AUC, indicating superior discriminative ability compared to individual features. The diagonal line represents a random classifier (AUC = 0.5). ROC, receiver operating characteristic.

cancer has significant advantages in predicting lung tumor infiltration.

The external validation of the prediction model was conducted using a separate dataset comprising 51 cases of multiple categories of lung nodules. The model performance was also evaluated using the ROC curve, which yielded an AUC of 0.856 (►**Fig. 5**). This indicates a strong discriminatory ability of the model to distinguish between invasive and noninvasive lung nodules. The model achieved a sensitivity of 0.80 and a specificity of 0.86, indicating a well-balanced performance between correctly identifying invasive nodules and minimizing false positives.

Discussion

Lung cancer stands as one of the most prevalent malignancies globally. The widespread adoption of chest CT scans has led to a steady rise in lung cancer detection rates over recent years. Findings from the 2011 National Lung Screening Trial underscore the efficacy of low-dose spiral CT in identifying up to 85% of stage I lung cancer cases, thereby enhancing patient survival by 20%.[9] However, as our comprehension of lung nodules deepens, concerns regarding overdiagnosis and overtreatment have gained prominence. Scholars abroad[10] have emphasized that the risk of overtreatment arises from challenges in accurately discerning the invasiveness of lung cancer. Misclassifying indolent tumors as aggressive ones can result in unwarranted interventions. Given the ambiguity surrounding pulmonary nodules, there exists controversy regarding the optimal timing for surgical intervention.[11,12] Hence, there is an urgent need to precisely differentiate between preinvasive and invasive lesions in clinical practice. Li et al[13] developed a model that effectively distinguishes between different stages of lung adenocarcinomas by integrating CT morphological features and nodule quantification parameters, thereby enhancing diagnostic accuracy. While blood-based tumor markers like CEA, NSE, cytokeratin 19 fragment (CYFRA21-1), Pro-GRP, and SCC are commonly used in diagnostic evaluations, their limited sensitivity and specificity restrict their utility as early-stage biomarkers.[14] In contrast, lung cancer autoantibodies have emerged as promising diagnostic indicators, detectable months or even years before cancer diagnosis through imaging tests.[15] This study endeavors to devise a predictive model leveraging CT features and seven lung cancer autoantibodies, aided by AI, to assess the invasiveness of lung cancer tumors.

The investigation unveiled several significant determinants influencing the invasiveness of lung cancer. Among

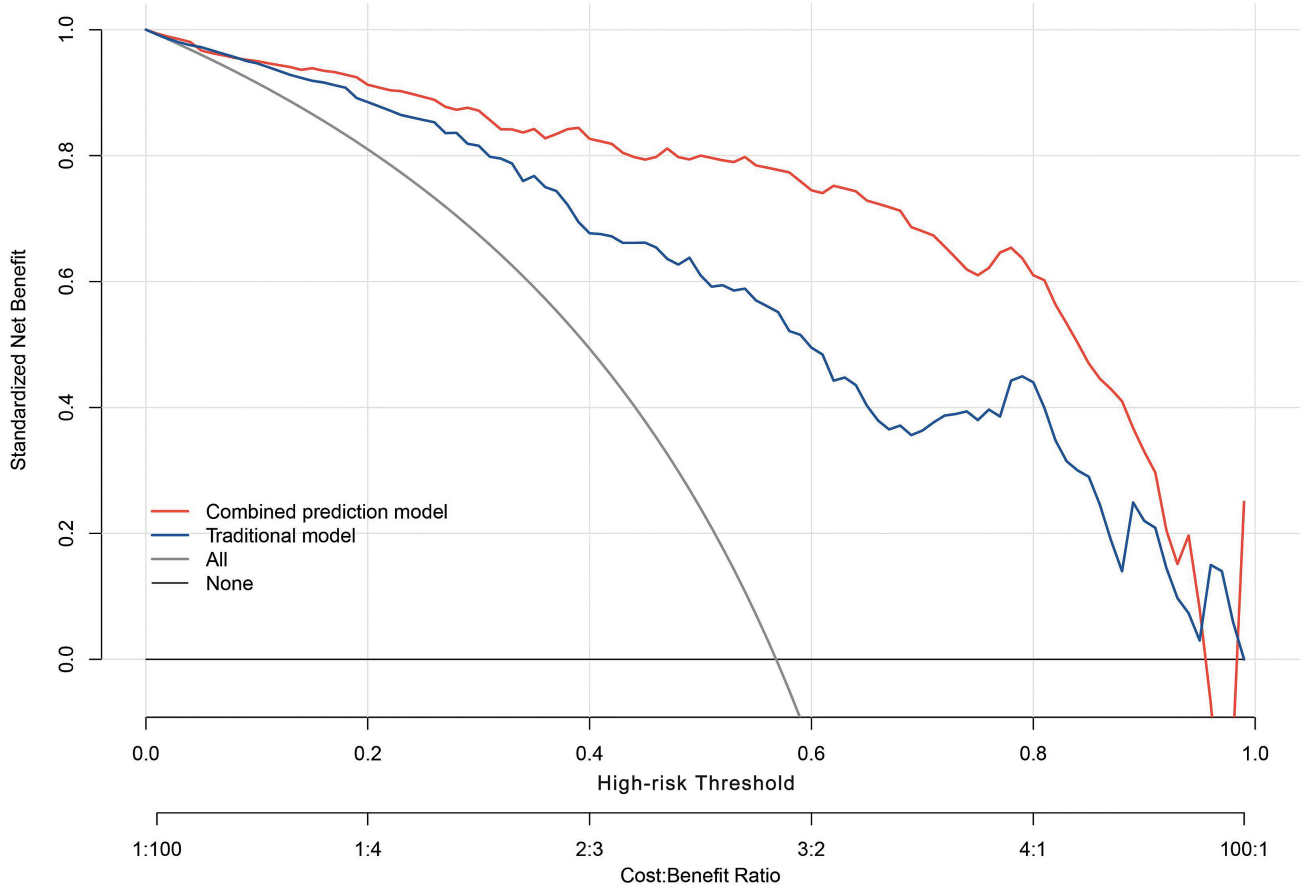

Fig. 3 decision curve analysis (dca) for the combined prediction model versus the traditional model. This DCA compares the standardized net benefit of the combined prediction model (orange line) and the traditional model (blue line) across different high-risk thresholds. The "All" (gray line) assumes that all patients are treated as having malignant nodules, while the "None" (black line) assumes that no patients are treated. The combined model shows a higher net benefit than the traditional model across a wide range of threshold probabilities, indicating superior clinical utility. The x-axis represents the high-risk threshold, and the y-axis represents the standardized net benefit.

these factors, the presence of lobulation sign, bronchial inflation sign, AI-predicted malignancy probability, partial solid nodule nature, nodule diameter, proportion of solid components, VEGF, and the presence of seven lung cancer autoantibodies emerged as independent risk factors. Notably, the proportion of solid components exhibited the highest discriminatory value in evaluating the invasiveness of lung cancer.

According to relevant studies,[16,17] certain conventional CT features, such as lobulation, spiculation, pleural indentation, and vascular convergence, exhibit significantly higher frequencies in invasive nodules compared to preinvasive ones. However, in the present study, only the presence of the lobulation sign and bronchial inflation sign demonstrated statistical significance in predicting tumor infiltration. Regarding tumor biomarkers, none showed statistical significance in predicting tumor infiltration, suggesting their limited capacity in determining nodule pathology. VEGF, a pivotal angiogenic factor, is implicated in lung cancer angiogenesis, tumor proliferation, and metastasis. While VEGF holds diagnostic value for lung cancer, it lacks associations with tissue type and clinical staging.[18] Among emerging tumor biomarkers, the seven autoantibodies for early lung cancer diagnosis exhibit notably higher sensitivity compared to traditional markers.[19] Their amalgamation with chest CT enhances the positive predictive value and diagnostic accuracy of malignant nodules, reducing the false positive rate of the autoantibodies.[20,21] In this study, the seven lung cancer autoantibodies emerged as significantly superior independent risk factors for predicting lung cancer invasiveness compared to other tumor markers. With the rapid advancement of technology, AI has become a cornerstone of technological progress in various industries, significantly expediting the medical technology revolution. AI facilitates the intuitive extraction of pulmonary nodule imaging features and can predict nodule malignancy probability through specific algorithms. Nevertheless, some scholars posit[22,23] that while AI can furnish ancillary evidence for clinical diagnosis, it cannot wholly replace human judgment.

The external validation results of the prediction model further reinforce its robustness and clinical utility. The model demonstrated a strong discriminatory ability to distinguish between invasive and noninvasive lung nodules with an AUC of 0.856, underscoring its potential application in clinical settings. The optimal threshold, identified by maximizing Youden's Index, provided a well-balanced sensitivity of 0.80 and specificity of 0.86. This balance suggests that the model

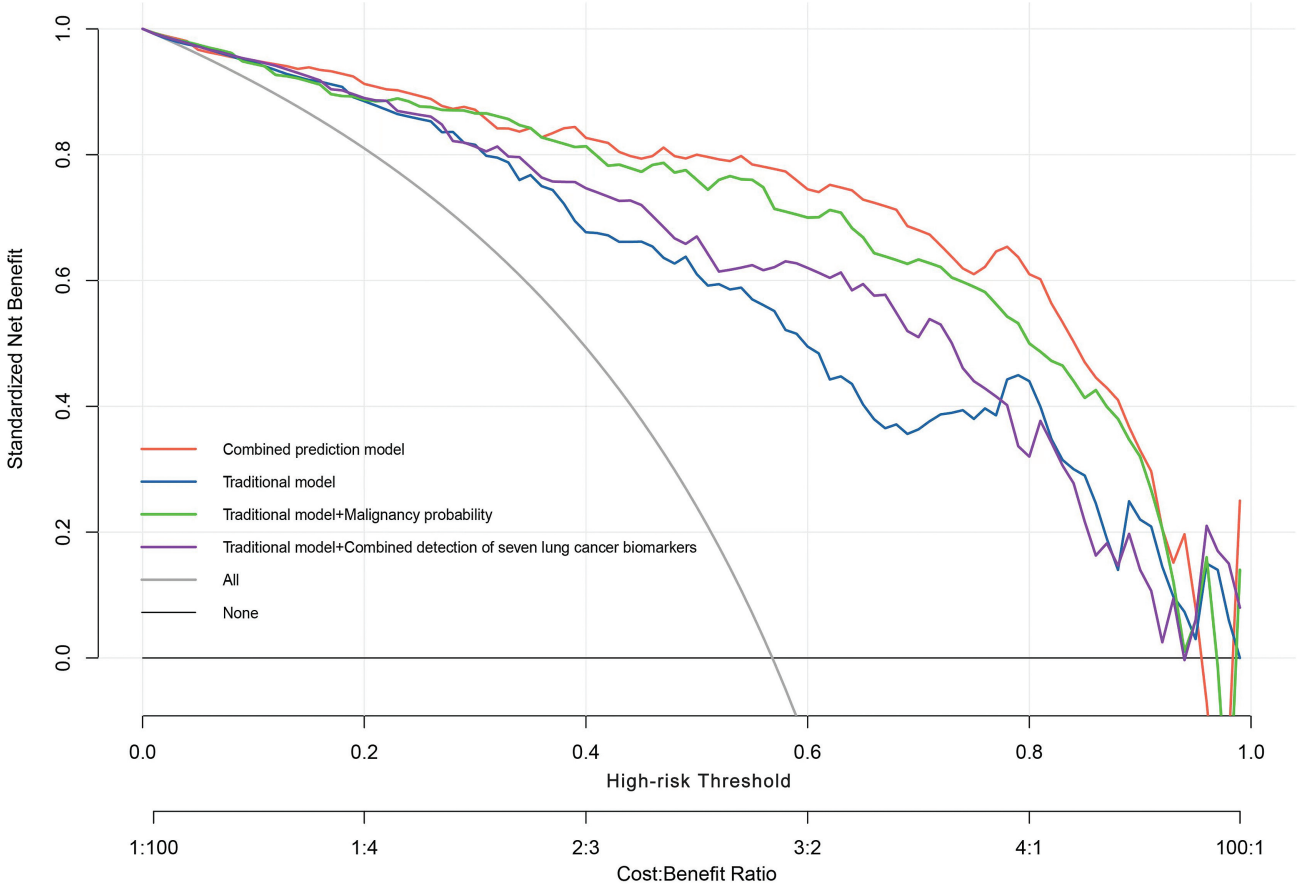

Fig. 4 decision curve analysis (dca) comparing various predictive models for lung nodule malignancy. This DCA evaluates the standardized net benefit of four predictive models across different high-risk thresholds: the combined prediction model (orange line), the traditional model (blue line), the traditional model combined with AI-predicted malignancy probability (green line), and the traditional model combined with the detection of seven lung cancer biomarkers (purple line). The "All" (gray line) assumes that all patients are treated as having malignant nodules, while the "None" (black line) assumes that no patients are treated. The combined model consistently provides the highest net benefit across a wide range of threshold probabilities, indicating superior clinical utility. The x-axis represents the high-risk threshold, and the y-axis represents the standardized net benefit. AI, artificial intelligence.

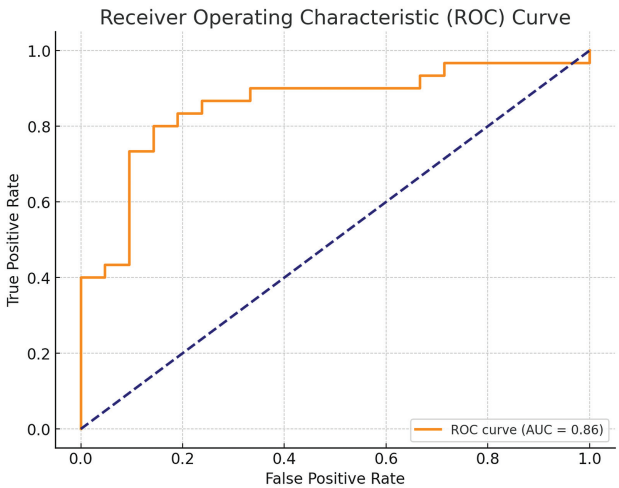

Fig. 5 ROC curve for external validation of the prediction model. The ROC curve represents the performance of the prediction model in distinguishing between invasive and non-invasive lung nodules using an external validation dataset of 51 cases. The model achieved an AUC of 0.856, indicating strong discriminatory power. The model's sensitivity was 0.80, and its specificity was 0.86. The diagonal line represents a random classifier (AUC = 0.5). AUC, area under the curve; ROC, receiver operating characteristic.

is effective not only in correctly identifying invasive nodules but also in minimizing false positive results, which is crucial for reducing unnecessary interventions and optimizing patient management. These findings highlight the model's potential for aiding clinical decision-making, particularly in scenarios where accurate risk stratification is critical. By integrating AI with CT features and lung cancer autoantibody detection, the model offers a novel, data-driven approach to assessing lung nodule invasiveness, thereby enhancing diagnostic precision and supporting personalized treatment strategies. Future research should focus on expanding the dataset and conducting further external validations to ensure the model's generalizability and to refine its predictive capabilities across diverse patient populations.

Conclusion

This combined approach of AI-based CT features analysis with lung cancer biomarkers provides a more accurate and clinically useful tool for guiding treatment decisions in pulmonary nodule patients. Further studies with larger cohorts are warranted to validate these findings across diverse patient populations.

Funding
This study was supported by Suzhou City Clinical Key Disease Diagnosis and Treatment Technology Special Project, LCZX202124.

Conflict of Interest
None declared.

References

1 Bray F, Ferlay J, Soerjomataram I, Siegel RL, Torre LA, Jemal A. Global cancer statistics 2018: GLOBOCAN estimates of incidence and mortality worldwide for 36 cancers in 185 countries. CA Cancer J Clin 2018;68(06):394–424
2 Chen W, Zheng R, Baade PD, et al. Cancer statistics in China, 2015. CA Cancer J Clin 2016;66(02):115–132
3 Kauczor HU, Bonomo L, Gaga M, et al; European Society of Radiology (ESR) European Respiratory Society (ERS) ESR/ERS white paper on lung cancer screening. Eur Radiol 2015;25(09):2519–2531
4 Li Q, Dai J, Zhang P, Jiang G. Management of pulmonary ground glass nodules: less is more. Ann Thorac Surg 2021;112(01):1–2
5 Zhang T, Zhang DG, Li J, et al. Real-world data analysis of artificial intelligence imaging system in the diagnosis of lung nodules. Sichuan Medicine 2021;42:193–196
6 Alpert JB, Lowry CM, Ko JP. Imaging the solitary pulmonary nodule. Clin Chest Med 2015;36(02):161–178, vii
7 Zhang RS, Zhang MF, Gao SG, et al. Interpretation of the change in the classification of lung adenocarcinoma in situ in the WHO classification of thoracic tumors in the fifth edition. Chin J Clin Thorac Cardiovasc Surg 2021;28:1012–1015
8 Ren S, Zhang S, Ma Z, et al. Validation of autoantibody panel for early detection of lung cancer in Chinese population. J Clin Oncol 2015;33:e22143–e22143
9 Aberle DR, Adams AM, Berg CD, et al; National Lung Screening Trial Research Team. Reduced lung-cancer mortality with low-dose computed tomographic screening. N Engl J Med 2011;365(05):395–409
10 Yankelevitz DF, Henschke CI. Overdiagnosis in lung cancer screening. Transl Lung Cancer Res 2021;10(02):1136–1140
11 MacMahon H, Naidich DP, Goo JM, et al. Guidelines for management of incidental pulmonary nodules detected on CT images: from the Fleischner Society 2017. Radiology 2017;284(01):228–243
12 Naidich DP, Bankier AA, MacMahon H, et al. Recommendations for the management of subsolid pulmonary nodules detected at CT: a statement from the Fleischner Society. Radiology 2013;266(01):304–317
13 Li X, Zhang W, Yu Y, et al. CT features and quantitative analysis of subsolid nodule lung adenocarcinoma for pathological classification prediction. BMC Cancer 2020;20(01):60
14 Tang ZM, Ling ZG, Wang CM, Wu YB, Kong JL. Serum tumor-associated autoantibodies as diagnostic biomarkers for lung cancer: a systematic review and meta-analysis. PLoS One 2017;12(07):e0182117
15 Tanoue LT, Tanner NT, Gould MK, Silvestri GA. Lung cancer screening. Am J Respir Crit Care Med 2015;191(01):19–33
16 Si MJ, Tao XF, Du GY, et al. Thin-section computed tomography-histopathologic comparisons of pulmonary focal interstitial fibrosis, atypical adenomatous hyperplasia, adenocarcinoma in situ, and minimally invasive adenocarcinoma with pure ground-glass opacity. Eur J Radiol 2016;85(10):1708–1715
17 Fan L, Liu SY, Li QC, Yu H, Xiao XS. Multidetector CT features of pulmonary focal ground-glass opacity: differences between benign and malignant. Br J Radiol 2012;85(1015):897–904
18 Trapé J, Buxó J, de Olaguer JP. Serum concentrations of vascular endothelial growth factor in advanced non-small cell lung cancer. Clin Chem 2003;49(03):523–525
19 Du Q, Yu R, Wang H, et al. Significance of tumor-associated autoantibodies in the early diagnosis of lung cancer. Clin Respir J 2018;12(06):2020–2028
20 Ren S, Zhang S, Jiang T, et al. Early detection of lung cancer by using an autoantibody panel in Chinese population. OncoImmunology 2017;7(02):e1384108
21 Zhong L, Coe SP, Stromberg AJ, Khattar NH, Jett JR, Hirschowitz EA. Profiling tumor-associated antibodies for early detection of non-small cell lung cancer. J Thorac Oncol 2006;1(06):513–519
22 Li Y, Chen D, Wu X, Yang W, Chen Y. A narrative review of artificial intelligence-assisted histopathologic diagnosis and decision-making for non-small cell lung cancer: achievements and limitations. J Thorac Dis 2021;13(12):7006–7020
23 Yeh MC, Wang YH, Yang HC, Bai KJ, Wang HH, Li YJ. Artificial intelligence-based prediction of lung cancer risk using nonimaging electronic medical records: deep learning approach. J Med Internet Res 2021;23(08):e26256

